Accepted Manuscript

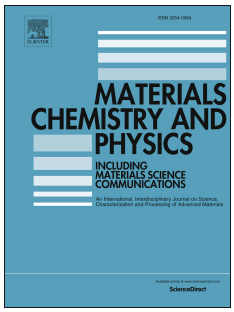

Electroless decoration of cellulose paper with nickel nanoparticles: A hybrid carbon fiber for supercapacitors

Xin Zhao, Honglei Chen, Shoujuan Wang, Qin Wu, Nannan Xia, Fangong Kong

PII: S0254-0584(18)30420-6

DOI: 10.1016/j.matchemphys.2018.05.024

Reference: MAC 20639

To appear in: *Materials Chemistry and Physics*

Please cite this article as: Xin Zhao, Honglei Chen, Shoujuan Wang, Qin Wu, Nannan Xia, Fangong Kong, Electroless decoration of cellulose paper with nickel nanoparticles: A hybrid carbon fiber for supercapacitors, *Materials Chemistry and Physics* (2018), doi: 10.1016/j.matchemphys.2018.05.024

Electroless decoration of cellulose paper with nickel nanoparticles: A hybrid carbon fiber for supercapacitors

Xin Zhao*, Honglei Chen, Shoujuan Wang, Qin Wu, Nannan Xia, Fangong Kong*

Key Laboratory of Pulp and Paper Science and Technology of Ministry of Education (Shandong Province), Qilu University of Technology (Shandong Academy of Sciences), Jinan 250353, P.R. China

*Corresponding authors: Xin Zhao, Fangong Kong. Tel/Fax: +86-0531-89631168.

E-mail: zhaoxin_zixi@126.com (Xin Zhao), kfg@qlu.edu.cn (Fangong Kong)

Abstract: A facile scale-up process was used to fabricate a novel hybrid carbon fiber material decorated with nickel nanoparticles for use as a supercapacitor electrode. Biomass-derived soft wood was transformed into cellulose fibers via papermaking technology. The cellulose fibers were then decorated with nickel nanoparticles via electroless decoration. The hybrid carbon fiber material was obtained by subsequent carbonization at 700 °C. The hybrid carbon fiber material exhibited promising capacitive performance as an electrode, showing a high specific capacitance of 268 F/g in 6 M KOH at a current density of 0.2 A/g, and excellent electrochemical stability of 97% capacity retention after 2000 cycles because of the synergistic effects of EDLC (carbon with a high specific surface area) and pseudocapacitor (slightly redox reaction) features.

Keywords: cellulose paper; electroless decoration; carbon fiber; supercapacitors

1. Introduction

To face the growing energy demand and environmental concerns, high-performance, cost-effective, and environmentally friendly energy storage and production systems are urgently required [1, 2]. Supercapacitors have attracted considerable attention as a promising new type of electrochemical device with high power density, excellent cycling performance, and low environmental pollution [3-5]. Generally, supercapacitors can be divided into electric double-layer capacitors (EDLCs) and pseudocapacitors. EDLCs accumulate charges via electrostatic force at the electrode/electrolyte interface. Pseudocapacitors exhibit fast and reversible Faradic processes between electrodes and electrolytes [6-8]. Combining these two mechanisms to optimize the performance of supercapacitors possesses obvious application prospects. Carbon materials such as carbon nanotubes [9], carbon spheres [10], and carbon fiber [11] play promising roles in EDLCs [12]. This is because these materials exhibit favorable electrochemical performance as a result of their high surface area, tunable pore size, and good electrical conductivity.

Carbon fiber exhibits extraordinary combined properties as stable structure and high porosity, a direct consequence of its highly oriented graphitic microstructure. However, the precursors used to prepare carbon fiber usually include fossil fuel derivates and polymers, which are unsuitable for large-scale synthesis because of their limited reserves. The development of green, and renewable energy sources for efficient energy storage systems is strongly desired. Biomass is recyclable and

abundant, and has been allotted numerous roles in sustainable development [13-15]. However, it is difficult to prepare carbon materials from wood without transformation technology because of its complicated structure. Papermaking technology provides an ideal platform for self-assembly of biomass-derived materials with three-dimensional hierarchical porous fiber structure, abundant functional groups, and hydrophilic properties. Also, paper is an ideal candidate substrate for flexible supercapacitor applications because it can be easily combined with a large variety of electrochemically active substances like conducting polymers. Moreover, metal can be deposited on common cellulose paper by the simple, low-cost electroless decoration method [16], leading to the formation of flexible and highly conductive hybrid carbon materials for use in supercapacitors. Electroless decoration is an environmentally friendly surface treatment technology that exhibits the advantages of low cost, simple equipment, uniform coating structure, strong bonding force, and high efficiency. However, despite the high efficiency and low-cost of electroless decoration, the activation process before plating plays an important role in this process, and improving supercapacitor performance with a low metal loading is also a challenge. Inspired by the above-mentioned ideas, we decided to use a combination of papermaking and electroless decoration to produce supercapacitor electrode materials with optimized performance.

In this study, we transform wood to cellulose fiber using mature papermaking technology. The cellulose fibers are decorated with nickel (Ni) nanoparticles via electroless deposition and then activated at high temperature to obtain a carbon fiber–

Ni nanoparticle hybrid material. The performance of this hybrid materials as a supercapacitor electrode is evaluated.

2. Experimental

2.1. Preparation of carbon fiber decorated with nickel nanoparticles

The cellulose paper was prepared based on reported papermaking technology [17]. In a typical process, lignin was partly removed from soft wood by adding sodium hydroxide (NaOH) and sodium sulphide (Na_2S). The sample was further digested at 175 °C for 2 h with a liquor ratio of 1:5 to separate the cellulose from the wood and leave softwood pulp. The wood pulp was washed, screened to remove large impurities, and then purified to remove heavy impurities. Finally, cellulose paper was obtained after papermaking and drying. Subsequently, the cellulose paper covered with Pd nanoparticles via an activation method ($Sn^{2+} + Pd^{2+} \rightarrow Sn^{4+} + Pd$) [18], which acted as seeds for Ni deposition. First, the cellulose paper was immersed in a sensitization solution consisting of 4 mM stannous chloride ($SnCl_2$) and 60 mM trifluoroacetic acid (TFA) in ethanol (3.3 mL) and deionized water (6.7 mL) for 5 min. The paper was thoroughly washed with ethanol/water solution (v:v=1:2), transferred to an activation solution consisting of 5 mM $PdCl_2$ and 80 mM NaCl in deionized water (10 mL) for 5 min, and then washed with ethanol/water solution again. The cellulose paper was washed with water and immersed in a plating bath containing $NiSO_4 \cdot 6H_2O$ (281 mg), $Na_3C_6H_5O_7 \cdot 2H_2O$ (294 mg), dimethylamine borane (DMAB; 59 mg), and deionized water (10 mL). Ni deposition was performed at room temperature for 1 h. *The hybrid carbon fiber–Ni* was formed after the sample was dried and carbonized under a N_2

atmosphere at 700 °C for 2 h, as shown in Fig. 1. For comparison, *carbon fiber* and *hybrid carbon fiber* samples were obtained from cellulose paper and hybrid cellulose paper, respectively, without sensitization and by activation under the conditions described above.

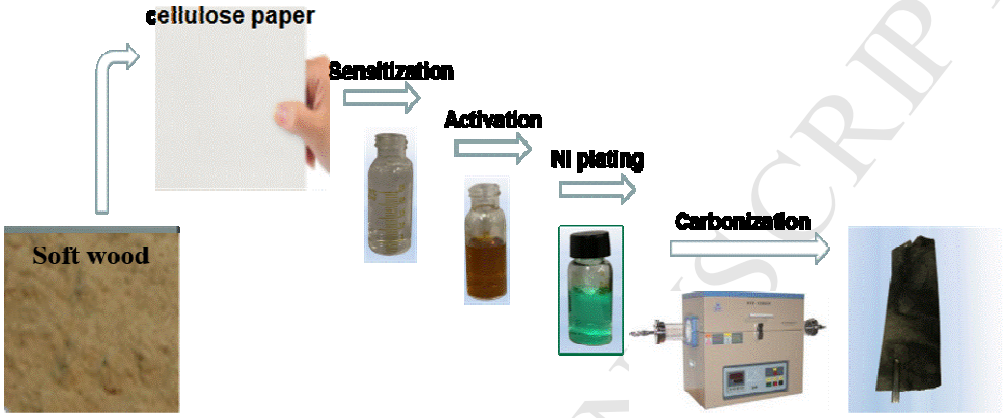

Fig. 1. Synthesis of hybrid carbon fibers with Ni nanoparticles

2.2. Characterization

Scanning electron microscopy (SEM) was performed using a JSM-7401F microscope (JEOL, Japan) at an acceleration voltage of 10 kV. Transmission electron microscopy (TEM) images were obtained on a JEOL 2011 apparatus (FEI, Holland) operated at 200 kV. Powder X-ray diffraction (XRD) patterns of samples were measured using a Bruker D4 (Bruker, Japan) powder X-ray diffractometer with Cu Kα radiation at 40 kV and 40 mA. Nitrogen sorption isotherms were measured with a Micromeritics ASAP 2020 sorptometer (Maike, USA) using N_2 as the adsorbate at 77 K. All samples were degassed at 300 °C for more than 10 h before analysis. The surface area (S_{BET}) was calculated from adsorption data in the relative pressure (P/P_0) range of 0.05–0.2 using the Brunauer–Emmett–Teller (BET) method, and total pore volume was determined at the highest P/P_0.

2.3. Electrochemical measurements

To fabricate electrodes, a carbon fiber sample, commercial carbon black, and polytetrafluoroethylene with a mass ratio of 8:1:1 were homogeneously mixed and then pressed on nickel foam. The typical mass of active materials on each electrode was about 5 mg. The electrochemical experiments were conducted in a three-electrode cell using a saturated calomel electrode (0.2415 V vs. the standard hydrogen electrode) as the reference electrode, a platinum plate as the counter electrode, the fabricated electrode as the working electrode, and 6 M KOH aqueous solution as the electrolyte. Cyclic voltammetry (CV) and electrochemical impedance spectroscopy (EIS) measurements were conducted using a PARSTAT 4000A (Princeton, USA) electrochemical workstation. CV curves were collected between −1 and 0 V at a scan rate of 100 mV/s. The EIS measurements were performed in the range from 10 mHz to 10 kHz with an AC amplitude of 5 mV. Galvanostatic charge/discharge tests were also performed using the PARSTAT 4000A electrochemical workstation at different current densities. The specific capacitance *Cg* (F/g) was calculated from $Cg = I\Delta t/m\Delta V$, where I (A) is the discharge current, Δt (s) is the discharge time, m (g) is the active mass of carbon material, and ΔV (V) is the potential window.

3. Results and discussion

The thermogravimetric analysis of cellulose paper and hybrid fiber–Ni samples were conducted (Fig. 2). The 5% weight loss temperature for cellulose paper was 250 °C (Fig. 2a), corresponding to the evaporation of water and small molecules [19]. At 380 °C, the sample weight loss reached 75%, which is typically attributed to the

decomposition of the constituents of cellulose paper, including some lignin, mostly hemicellulose, and cellulose; for example, the decomposition of aromatic rings and methylene groups, and the release of different polysaccharides/monosaccharides [18, 19]. Further raising the temperature to >650 °C did not strongly affect the material; the residual mass loss of 10% was attributed to the decomposition of heavy impurities [19]. In contrast, the hybrid carbon fiber–Ni displayed a rapid weight loss at 395 °C (Fig. 2b), which might be caused by the decomposition of nitrate salt to nickel and nickel oxides and volatile gases (H_2O, sulfide gas) during carbonization. The residual mass of the carbon hybrid fiber–Ni was 52% (carbon ash accounts for 10% of this). This result indicates that the Ni metal was stably attached to the carbon fibers, and nickel and nickel oxide accounted for 42% of the final sample. The mechanical properties of the final sample revealed its high stiffness, which is because it is composed of carbon and metal with high rigidity. The carbonization temperature for the samples was chosen based on the thermogravimetric analysis results for cellulose paper and the hybrid carbon fiber–Ni under N_2 (Fig. 2). Accordingly, we selected 700 °C as the carbonization temperature for the carbon fiber samples.

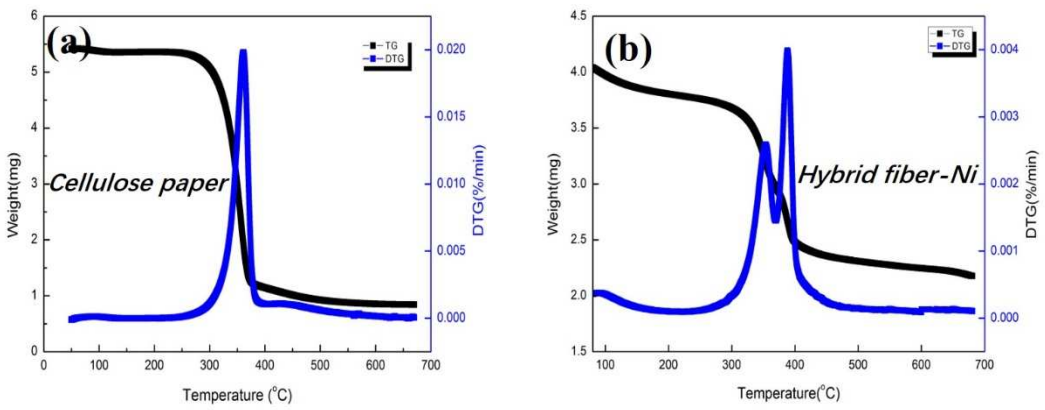

Fig. 2 Thermogravimetric analysis of (a) cellulose paper and (b) hybrid fiber–Ni

Powder XRD patterns of the samples are shown in Fig. 3. All samples displayed a broad diffraction peak at 24°, which represented the (002) lattice plane of graphitic carbon [20]. The hybrid carbon fiber–Ni exhibited a sharp peak at ca. 46° that indicated the presence of Ni (111) (JCPDS No. 04-0850) [21]. Because of the strong hydrogen-bonding interaction between the hydroxyl groups of cellulose and activation solution, Pd nanoparticles acted as seeds for Ni deposition on the cellulose paper surface [22]. The results showed that the sensitization and activation processes played important roles in the success of Ni plating of the hybrid sample. The XRD pattern of the hybrid sample contained another sharp peak at 57° that was consistent with the NiO (202) lattice plane (JCPDS No. 44-1159) [22, 23]. The reason for the presence of NiO is that NiO was not completely transformed to Ni ($NiO + C \rightarrow Ni + CO/CO_2$) during the carbonization process. However, the synergistic effect of Ni and NiO could improve the electrical conductivity of the hybrid carbon fiber–Ni [23]. The XRD pattern of the hybrid sample only contained major peaks from Ni and NiO, which may be because only a small amount Ni was introduced. However, a low metal loading is desirable to improve supercapacitor performance.

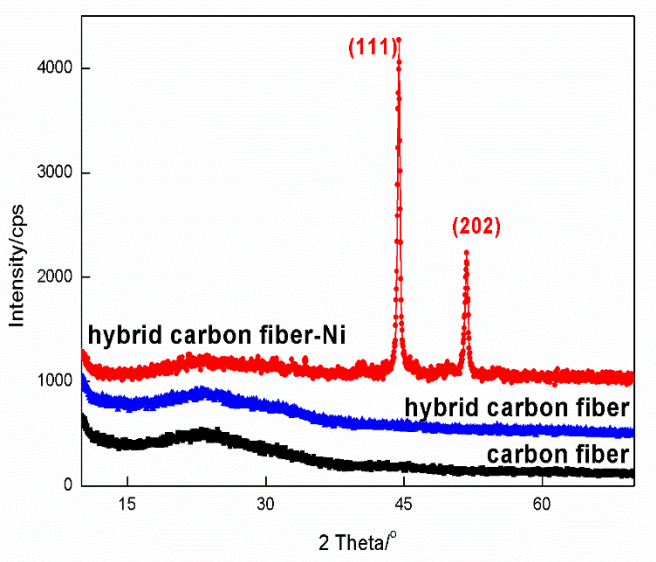

Fig. 3. Powder XRD patterns of carbon fiber, hybrid carbon fiber, and hybrid carbon fiber–Ni samples

The photographs in Fig. 4 reveal that the white cellulose paper (Fig. 4a) transformed to black upon carbonization (Fig. 4 d and g). The hybrid carbon fiber felt soft to the touch, but the hybrid carbon fiber–Ni sample did not. This change was attributed to Ni deposition, which was driven by the reduction reaction between DMAB and $NiSO_4$ [24, 25]. At low magnification (Fig. 4b, e, and h), the cellulose paper sample obtained via papermaking technology exhibited comparably smooth fibers (Fig. 4b), as did the hybrid carbon fibers (Fig. 4e). After sensitization and activation to form the hybrid carbon fiber–Ni, the surface of the fiber support was densely covered with a great number of Ni nanoparticles (Fig. 4h), causing the carbon surface to change from black to gray (Fig. 4d and g). The porous fiber skeleton structure of the paper was well maintained after electroless decoration. This result shows that cellulose paper is an ideal candidate substrate because it can be stably and easily combined with a large variety of electrochemically active substances [26]. The

well-distributed Ni nanoparticles were closely connected to the carbon fibers, indicative of their strong adhesion. TEM observations were executed to further study the structure of the different samples. As shown in Fig. 4c, the carbon fibers of the cellulose paper exhibited typical honeycomb-like pores. Disordered graphitic microstructure and some distorted lattice fringes were observed near the edges of the hybrid carbon fiber sample, representing graphene-type layers (Fig. 4f). Such a weakly ordered graphitic microstructure is beneficial to enhance electrical conductivity. Hybrid carbon fiber–Ni sample displays abundant crystal lattices (Fig. 4i). The tight packing of the Ni crystal lattice indicates the high nucleation density in the sample, which is probably related to the polar surface chemistry, and can be exploited to fabricate electrode materials containing Ni and NiO nanoparticles [27].

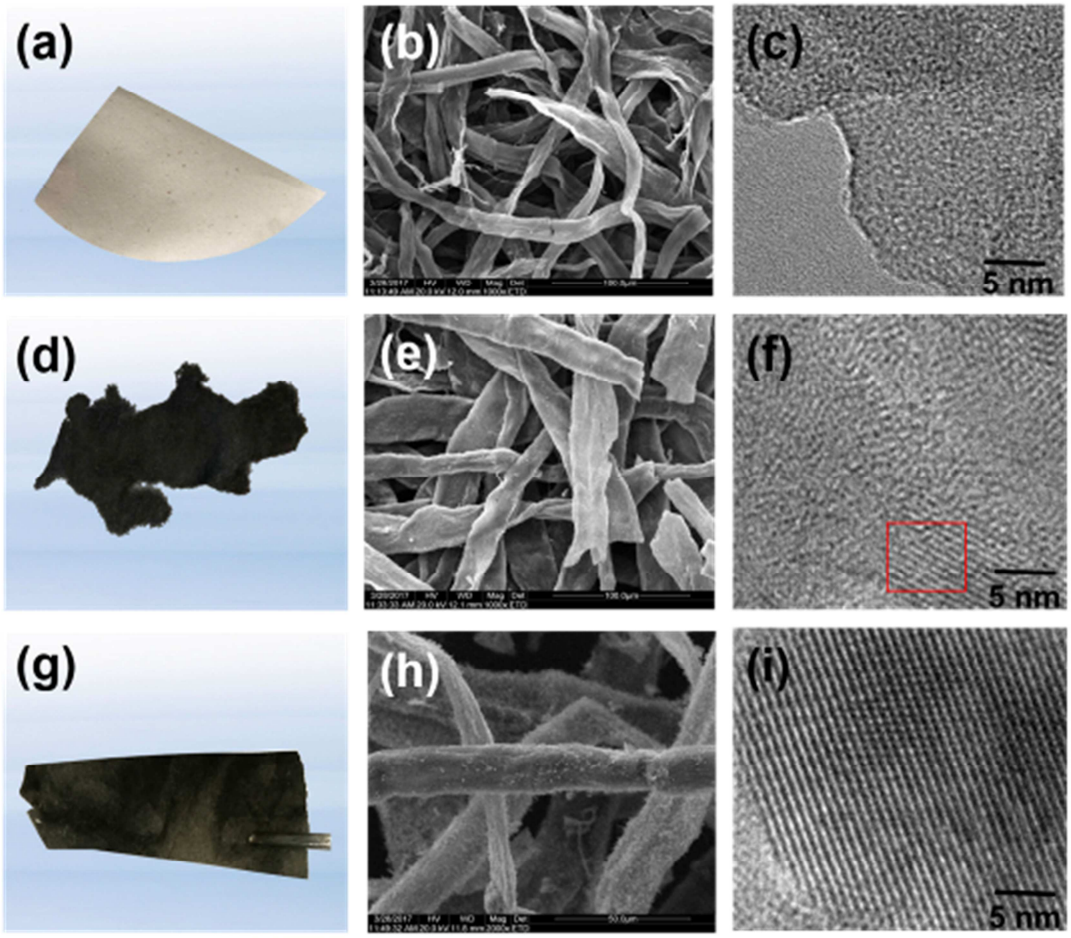

Fig. 4 Photographs of (a) carbon fiber, (d) hybrid carbon fiber, and (g) hybrid carbon fiber–Ni. SEM images of (b) carbon fiber, (e) hybrid carbon fiber, and (h) hybrid carbon fiber–Ni. TEM images of (c) carbon fiber, (f) hybrid carbon fiber, and (i) hybrid carbon fiber–Ni.

The porosity of the materials before and after Ni deposition were calculated according to [28]:

$$\text{Porosity} = (1 - \rho_{SG} / \rho_{bulk)} \times 100\%,$$

where ρ_{SG} and ρ_{bulk} are the density of the sponge and corresponding bulk density, respectively. The densities of carbon and nickel are 0.45–0.65 and 8.903 g/cm^3, respectively. The calculated porosity of the hybrid carbon fiber–Ni is 98.1%. This is

slightly higher than that of the carbon fiber is 97.3%, which is attributed to graphitization improved after Ni coating.

The nitrogen sorption isotherms and corresponding pore size distribution curves of the carbon fiber, hybrid carbon fiber, and hybrid carbon fiber–Ni are shown in Fig. 5. The isotherms can all be classified as mixed I–IV isotherms with steep adsorption below P/P_0 (Fig. 5a), indicating the presence of abundant micropores, and typical H_2 hysteresis loop at P/P_0 = 0.4–1, which is associated with capillary condensation in mesopores [29]. Carbon fiber has a low N_2 adsorption capacity at P/P_0 = 0.1, indicating its low micropore content. This sample shows representative type-IV isotherms with an H_4 hysteresis loop in the P/P_0 range of 0.4–1.0, illustrating that the carbon fiber is a typical mesoporous material. The hybrid carbon fiber has a high N_2 adsorption capacity at P/P_0 = 0.1, but the H_4 hysteresis loop in the P/P_0 range of 0.4–1.0 is similar to that of the carbon fiber, indicating the presence of much more micropores in the material after the hybridization process. The hybrid carbon fiber–Ni displayed a higher N_2 adsorption capacity at P/P_0 = 0.1 than those of the other samples, and its hysteresis loop in the P/P_0 range of 0.4–-1.0 was slightly changed from those of the other samples. These results indicated that the sample porosity improved sharply because of the formation of many more micropores and mesopores following hybridization and carbonization. Combined with the pore size distribution curves (Fig. 5b), showed that all of the samples exhibited pore sizes in the range of 1-3 nm. The mesoporous distribution and the number of micropores increased after Ni coating.

Table 1 summarizes the textural properties determined for the carbon fiber, hybrid carbon fiber, and hybrid carbon fiber–Ni. Pore formation in the carbon fiber samples was mainly caused by volatilization of small molecules derived from cellulose, hemicellulose, and lignin during the carbonization process [19]. S_{BET} of the hybrid carbon fiber–Ni (369 m^2/g) was higher than those of the carbon fiber (90 m^2/g) and hybrid carbon fiber (130 m^2/g). This is because more gas decomposed from the nickel salt (H_2O and sulfide) during Ni nanoparticle deposition [30]. The surface area increase from 130 to 369 m^2/g for the hybrid carbon fiber-Ni is caused by the introduction of a small amount of metal, which could also improve graphitization [30, 31]. The hybrid carbon fiber–Ni should contain more active groups that can contact with the electrolyte than the other samples, which should enhance its specific capacitance. The increase of S_{BET} and average pore size observed following the plating, sensitization, and activation processes is attributed to the Ni nanoparticles impeding the shrinkage of the carbon framework, resulting in more numerous and larger pores [32, 33].

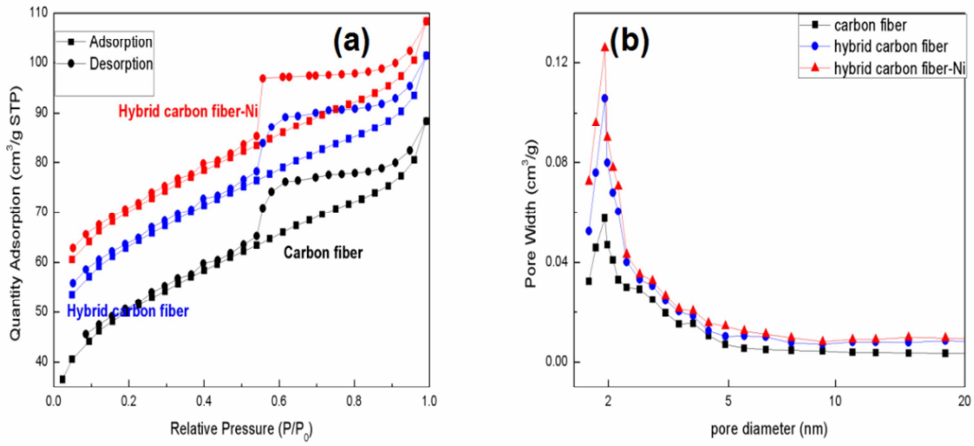

Fig. 5 (a) Nitrogen sorption isotherms and (b) pore size distribution of carbon fiber,

hybrid carbon fiber, and hybrid carbon fiber–Ni samples

Table.1 Textural parameters of the carbon fiber, hybrid carbon fiber, and hybrid carbon fiber–Ni samples

Sample	S_{BET} (m^2/g)	S_{meso}/S_{BET} (%)	V_{total} (cm^3/g)	Average Pore Size (nm)
Carbon fiber	90	30%	0.07	2.3
Hybrid carbon fiber	130	33%	0.10	2.7
Hybrid carbon fiber-Ni	369	37%	0.13	3.2

3.3. Electrochemical properties

The electrochemical properties of the samples were studied through CV, galvanostatic charge/discharge (GCD), and EIS measurements in a 6 M KOH aqueous electrolyte. CV curves for different samples measured with different scan rates (20, 50, and 100 mV/s) are presented in Fig. 6. The CV curve for the hybrid carbon fiber–Ni sample at low scan rate (Fig. 6c) contained a small redox reaction peak compared with those of the other samples. The presence of heteroatoms is not evident, which is because of the low nickel content. The electrochemical data for the hybrid carbon fiber–Ni sample are improved compared with those of the other samples because of the synergistic effect of its EDLC (carbon with a high specific surface area) and pseudocapacitor (slightly redox reaction) features [34]. As a result, the hierarchical porous hybrid carbon fiber–Ni sample exhibits excellent supercapacitance performance.

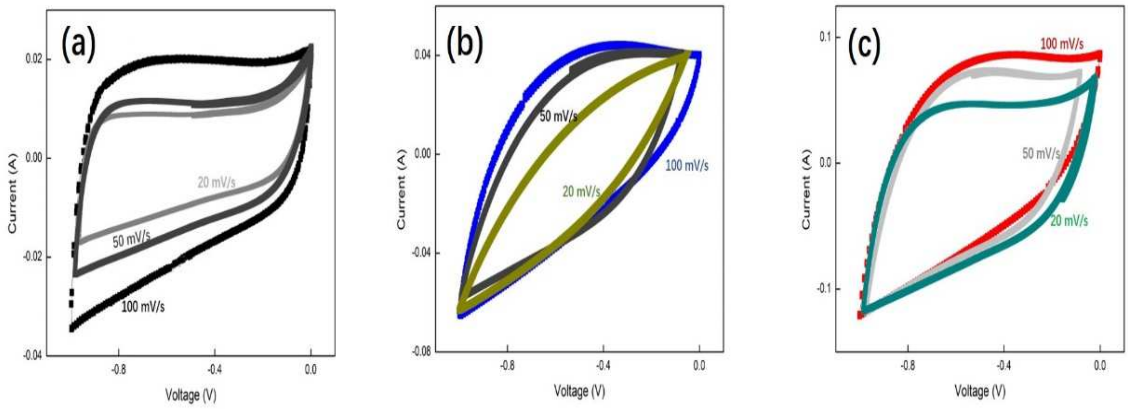

Fig. 6. CVs of (a) carbon fiber, (b) hybrid carbon fiber, and (c) hybrid carbon fiber–Ni samples measured at different scan rates (20, 50, and 100 mV/s)

Figure 7a compares the CV curves obtained for the carbon fiber, hybrid carbon fiber, and hybrid carbon fiber–Ni electrodes at 100 mV/s. All the CV curves display a roughly rectangular shape in the potential window of −0.1–0 V, indicating EDLC behavior [34]. However, the CV area of the carbon fiber is relatively small, implying low capacitance. Compared with those of the carbon fiber and hybrid carbon fiber electrodes, the CV area of hybrid carbon fiber–Ni electrode is markedly larger, which is caused by the contributions of both the EDLC effect of carbon and pseudocapacitance of Ni. It is obvious that the activation process is beneficial to improve the capacitance of the samples. Activation caused the Ni nanoparticles to attach to the fiber support [35].

The GCD curves of the three samples are shown in Fig. 7b. The hybrid carbon fiber–Ni showed GCD curves that were nearly isosceles triangles, revealing the excellent conductivity of this electrode material [36-38]. The superior conductivity of this electrode was attributed to the presence of Ni metal after sensitization and

activation via a simple method. The GCD plots of the hybrid carbon fiber–Ni electrode measured at current densities from 0.2 to 2 A/g are shown in Fig. 7c. The specific capacitance of the hybrid carbon fiber–Ni measured at a current density of 0.2 A/g was 268 F/g, and remained at 200 F/g when the current density was increased to 2 A/g, indicating the high conductivity of this sample, which was attributed to its well-defined porosity. The capacitance decreases of all the carbon samples observed at high current density was ascribed to the limited charge diffusion in the pores because of the time constraints of the charge/discharge process [39].

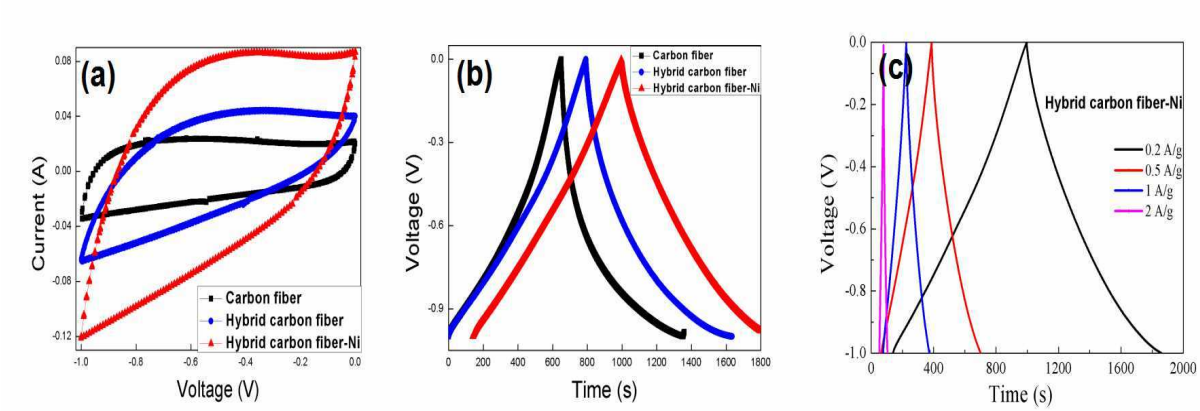

Fig. 7. (a) CV curves (scan rate of 100 mV/s) and (b) GCD curves (current density of 0.2 A/g) of carbon fiber, hybrid carbon fiber, and hybrid carbon fiber–Ni samples. (c) GCD curves of hybrid carbon fiber–Ni electrode (0.2–2 A/g)

To further investigate the electrochemical performance of the different samples, their cycling stability and EIS were systematically evaluated. The cycling stability tests of the electrodes were performed at a current density of 0.2 A/g for 2000 GCD cycles, as shown in Fig. 8a. The hybrid carbon fiber–Ni electrode displayed the highest charge–discharge stability of those investigated; its specific capacitance decreased only slightly, remaining above 97% of the initial capacitance after 2000

cycles. This result indicates that the hybrid carbon fiber–Ni electrode has good electrochemical stability and a high degree of reversibility because of its well-developed porosity [38].

The charge transfer and electrolyte diffusion at the electrode/electrolyte interface were evaluated by EIS. Figure 8b compares the Nyquist plots for the carbon fiber, hybrid carbon fiber, and hybrid carbon fiber–Ni electrodes. In the low frequency region, the hybrid carbon fiber–Ni electrode displayed the highest slope, indicating the lowest resistance and best capacitive behavior of the samples. The capacitive performance of the hybrid carbon fiber–Ni electrode is promising because Ni can easily transfer the activation energy to allow the rapid variation of the potential [39]. In the high frequency region, the capacitive behavior of the electrodes is illustrated by semicircular plots; a small semicircle indicates a low contact resistance, which is related to the interaction between the porous structure of the electrode and ions [40, 41]. The hybrid carbon fiber–Ni electrode displayed a semicircle with a smaller radius than those of the hybrid carbon fiber and carbon fiber electrodes, which was because of the Ni nanoparticles penetrating into the pores. At low frequency, a straight line in a Nyquist plot demonstrates the ideal EDLC behavior of an electrode material [42]. The low internal resistance increases conductivity. Because of the synergistic effect of high specific surface area and low pseudocapacitance, the hybrid carbon fiber–Ni electrode exhibits the highest slope in its Nyquist plot, indicating it has the lowest resistance of the electrodes and excellent supercapacitive performance. These results are consistent with the CV and GCD analyses. The hybrid carbon fiber–Ni electrode

has well-developed porosity, resulting in low resistance and excellent electrochemical performance [43-46], as shown by the comparison with other electrodes in Table 2. This carbon material is therefore a promising candidate for use in supercapacitors.

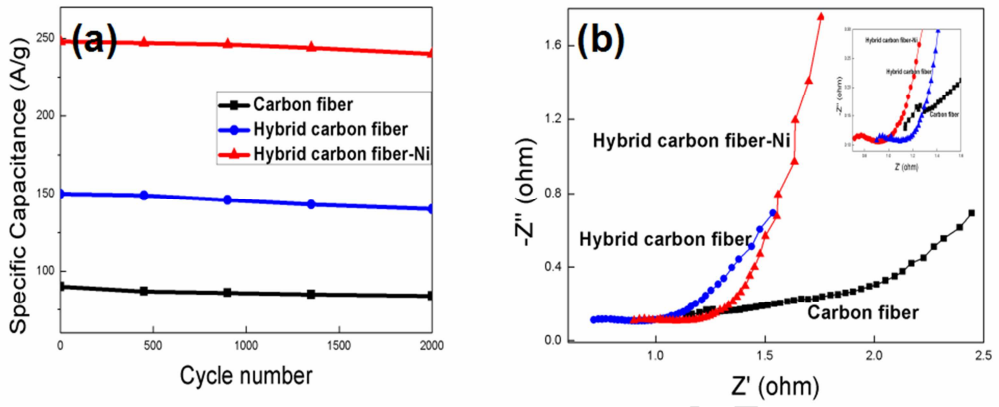

Fig. 8. (a) Cycling stability measured at 0.2 A/g and (b) Nyquist plots for the carbon fiber, hybrid carbon fiber, and hybrid carbon fiber–Ni samples.

Table. 2 Comparison of the specific capacitances of different nickel/carbon fiber materials

Sample	specific capacitance
Hybrid carbon fiber-Ni (this work)	268 F/g
Nickel/carbon nanofibers [43]	164 F/g
Nickel/carbon nanotube [44]	155 F/g
Carbon nanotubes-nickel oxide porous composite [45]	206 F/g
Nickel catalytic graphitized porous carbon [46]	248 F/g

4. Conclusions

We demonstrated a facile method to fabricate a hybrid material composed of carbon fiber with nickel nanoparticles from cellulose paper. Papermaking transformed the amorphous structure of soft wood to carbon fiber. Rough metal nanoparticles were

then deposited on the carbon fiber by electroless deposition. This approach only relied on intrinsic structuring mechanisms of randomly arranged fibers and metal nanoparticle deposition during electroless plating and subsequent carbonization at 700 °C. No complex multistep processes were required, only standard chemicals were used, and the support was synthesized from biomass, which is an abundant resource. Electroless decoration of the carbon fiber with nickel nanoparticles optimized the supercapacitive performance of the material. The hybrid material displayed a high specific capacitance of 268 F/g in 6 M KOH at a current density of 0.2 A/g, good cyclic stability with capacitance retention of 97% after 2000 cycles, outstanding conductance stability, and favorable mechanical flexibility. These results indicate that this flexible, highly conductive, and free-standing hybrid carbon fiber–Ni holds great promise as an electrode material to fabricate high-performance, flexible, and hand-held energy storage devices.

Acknowledgment

The present work was financially supported by the Natural Science Foundation of Shandong (ZR2017LEM009), the National Natural Science Foundation of China (Grant No. 31600472, 31570566, and 31500489), the Foundation of Key Laboratory of Pulp and Paper Science and Technology of Ministry of Education/Shandong Province of China (No. ZR201707 and ZR201710), the Key Research and Development Program of Shandong Province (No. 2017GSF17130), the Foundation of Guangxi Key Laboratory of Clean Pulp & Papermaking and Pollution Control of China (KF201717), and the Undergraduate Innovation and Entrepreneurship Program

of Qilu University of Technology (No: xj201710431007 and xj201710431009). We thank Natasha Lundin, from Liwen Bianji, Edanz Editing China (www.liwenbianji.cn/ac), for editing the English text of a draft of this manuscript.

References

[1] J. Li, C. Wang, P. Zheng, Solvothermal preparation of micro/nanostructured TiO 2 with enhanced lithium storage capability, Mater Chem Phys. 190 (2017) 202-208.

[2] A.C. Patsidis, K. Kalaitzidou, G.C. Psarras, Dielectric response, functionality and energy storage in epoxy nanocomposites: Barium titanate vs exfoliated graphite nanoplatelets, Mater Chem Phys. 135(2) (2012) 798-805.

[3] J.Y. Shieh, S.Y. Tsai, B.Y. Li, High-performance flexible supercapacitor based on porous array electrodes, Mater Chem Phys. 195 (2017) 114-122.

[4] L. Zhang, Z. Liu, X. Lu, G. Yang, Z.Y. Cheng, Nano-clip based composites with a low percolation threshold and high dielectric constant, Nano Energy, 26 (2016) 550-557.

[5] W.H. Xu, Y.C. Ding, Y. Yu, S.H. Jiang, L.L. Chen, H.Q. Hou, Highly foldable PANi@CNTs/PU dielectric composites toward thin-film capacitor application, Mater Lett. 192 (2017) 25-28.

[6] M. Zhang, L. Zhang, M. Zhu, Y.G. Wang, N.W. Li, Z.J. Zhang, Q. Chen, L.A. An, Y.H. Lin, C.W. Nan, Controlled functionalization of poly(4-methyl-1pentene) films for high energy storage applications, J. Mater. Chem. A 4 (2016) 4797-4807.

[7] Y.X. Li, P. Miao, W. Zhou, X. Gong, X.J. Zhao, N-doped carbon-dots for luminescent solar concentrators, J. Mater. Chem. A 5 (2017) 21452-21459.

[8] H. Zhuo, Y.J. Hu, X. Tong, L.X. Zhong, X.W. Peng, R.C. Sun, Sustainable hierarchical porous carbon aerogel from cellulose for high-performance supercapacitor and CO_2 capture, Ind. Crop. Prod. 87 (2016) 229-235.

[9] C. Fu, H. Zhou, R. Liu, Supercapacitor based on electropolymerized polythiophene and multi-walled carbon nanotubes composites, Mater Chem Phys. 132(2) (2012) 596-600.

[10] M.K. Seo, S. Yang S, I.J. Kim, Preparation and electrochemical characteristics of mesoporous carbon spheres for supercapacitors, Mater Res Bull. 45 (2010) 10-14.

[11] K. Huang, Y. Yao, X. Yang, Fabrication of flexible hierarchical porous nitrogen-doped carbon nanofiber films for application in binder-free supercapacitors, Mater Chem Phys. 169 (2016) 1-5.

[12] J. Chen, X. Zhou, C. Mei, Evaluating biomass-derived hierarchically porous carbon as the positive electrode material for hybrid Na-ion capacitors, J. Power Sources. 342 (2017) 48-55.

[13] A. Jain, R. Balasubramanian, M.P. Srinivasan, Hydrothermal conversion of biomass waste to activated carbon with high porosity: A review, Chem. Eng. J. 283 (2016) 789-805.

[14] C.X. Hu, S.J. He, S.H. Jiang, S.L. Chen, H.Q. Hou, Natural source derived carbon paper supported conducting polymer nanowire arrays for high

performance supercapacitors, RSC Adv. 5 (2015) 14441-14447.

[15] S.Z. Zhou, G.Y. Zhou, S.H. Jiang, P.C. Fan, H.Q. Hou, Flexible and refractory tantalum carbide-carbon electrospun nanofibers with high modulus and electric conductivity, Mater Lett. 200 (2017) 97-100.

[16] T. Qiu, P.K. Chu, Self-selective electroless plating: An approach for fabrication of functional 1D nanomaterials, Mat. Sci. Eng. R. 61 (2008) 59-77

[17] H. Koga, N. Namba, Y. Nishina, Renewable wood pulp paper reactor with hierarchical micro/nanopores for efficient continuous-flow nanocatalysis, ChemSusChem (2017) DOI: 10.1002/cssc.201700576.

[18] X. Zhao, F. Muench, S. Schaefer, J. Brötz, S.X. Liu, W. Ensinger, Electroless decoration of macroscale foam with nickel nano-spikes: A scalable route toward efficient catalyst electrodes, Electrochem. Commun. 65 (2016) 39-43.

[19] H. Peng, N. Wang, Z. Hu, Z. Yu, Y. Liu, J. Zhang, Physicochemical characterization of hemicelluloses from bamboo (Phyllostachys pubescens Mazel) stem. Indust. Crops. Prod. 37 (2012) 41-50.

[20] Y. Meng, A family of highly ordered mesoporous polymer resin and carbon structures from organic-organic self-assembly, Chem. Mater. 18 (2006) 4447-4464.

[21] K.S.W. Sing, Reporting physisorption data for gas/solid systems with special reference to the determination of surface area and porosity, Pure. Appl. Chem. 57 (1985) 603-619.

[22] Martin d'Halluin, Jordi Rull-Barrull, Guillaume Bretel, Chemically modified

cellulose filter paper for heavy metal remediation in water, ACS Sustain Chem. Eng. 5 (2017) 1965-1973.

[23] J. Wang, W. Zeng, Z.C. Wang, Assembly of 2D nanosheets into 3D flower-like NiO: Synthesis and the influence of petal thickness on gas-sensing properties, Ceram. Int, 42 (2016) 4567-4573.

[24] S. Arai, Y. Imoto, Y. Suzuki, M. Endo, Fabrication of Ni–B alloy coated vapor-grown carbon nanofibers by electroless deposition, Carbon 49 (2011) 1484–1490.

[25] T.C. Wei, T.C. Pan, C.M. Chen, K.C. Lai, C.H. Wu, Annealing-free adhesive electroless deposition of a nickel/phosphorous layer on a silane-compound-modified Si wafer, Electrochem. Commun. 54 (2015) 6–9.

[26] C.C. Wan, Y. Jiao, J. Li, Flexible, highly conductive, and free-standing reduced graphene oxide/polypyrrole/cellulose hybrid paper for supercapacitor electrodes, J. Mater. Chem. A. 2013, 1-3.

[27] K.A. Nelson, M.R. Linford, D.R.Wheeler, J.N. Harb, Use of a plating additive to enable continuous metallization of nanoscale electrochemically patterned chemical templates, Electrochem. Acta. 69 (2012) 320–327.

[28] S.H. Jiang, G.G. Duan, U. Kuhn, M. Mörl, V. Altstädt, A.L. Yarin, A. Greiner, Spongy Gels by a Top-Down Approach from Polymer Fibrous Sponges. Angew. Chem. Int. Edit. 56 (2017) 3285-3288.

[29] C.H. Huang, R.A. Doong, Sugarcane bagasse as the scaffold for mass production of hierarchically carbon monoliths by surface self-assembly. Microporous

Mesoporous Mater. 147 (2012) 47-52.

[30] R. Fu, T.F. Baumann, S. Cronin, G. Dresselhaus, M.S. Dresselhaus, Formation of graphitic structures in cobalt-and nickel-doped carbon aerogels, Langmuir the Acs Journal of Surfaces & Colloids, (2005) 2647-2651.

[31] M. Liu, L. Gan, W. Xiong, F. Zhao, X. Fan, Nickel-doped activated mesoporous carbon microspheres with partially graphitic structure for supercapacitors, Energy & Fuels, 27 (2013) 1168-1173.

[32] L. Zubizarreta, A. Arenillas, J.J. Pis, Preparation of Ni-doped carbon nanospheres with different surface chemistry and controlled pore structure, Appl Surf Sci, 254 (2008) 3993-4000.

[33] T. Liu, C. Jiang, B. Cheng, W. You, J. Yu, Hierarchical flower-like C/NiO composite hollow microspheres and its excellent surpercapacitor performance, J. Power Sources, 359 (2017) 371-378.

[34] O. Martin, B. Sofiane, N. Winfried, Jan P. Hofmann, Carbide-derived carbon aerogels with tunable pore structure as versatile electrode material in high power supercapacitors, Carbon 113 (2017) 283-291.

[35] N. Mao, H.L. Wang, Y. Sui, D. Mitlin, Extremely high-rate aqueous supercapacitor fabricated using doped carbon nanoflakes with large surface area and mesopores at near-commercial mass loading, Nano Research. 10 (2017) 1767-1783.

[36] W.L. Zhang, C. Xu, C.Q. Ma, G.X. Li, Y.Z. Wang, N.J. Tang, W.C. Ren, Nitrogen-superdoped 3D graphene networks for high-performance

supercapacitors, Adv. Mater. (2017) 1701677.

[37] X. Zhao, S.J. Wang, Q. Wu, Nitrogen and phosphorus dual-doped hierarchical porous carbon with excellent supercapacitance performance, Electrochim. Acta, 247 (2017) 1140-1146.

[38] T. Thomberg, A. Jänes, E. Lust, Energy and power performance of electrochemical double-layer capacitors based on molybdenum carbide derived carbon, Electrochim. Acta. 55 (2010) 3138-3143.

[39] C. Lei, P. Wilson, C. Lekakou, Effect of poly (3,4-ethylenedioxythiophene) (PEDOT) in composite electrodes for electrochemical supercapacitors, J. Power. Sources. 196 (2011) 7823-7827.

[40] X. Du, W. Zhao, Y. Wang, C. Wang, M. Ma, Preparation of activated carbon hollow fibers from ramie at low temperature for electric double-layer capacitor applications, Bioresource Technol. 149 (2013) 31-37.

[41] W.J. Liu, K. Tian, L.L. Ling, H.Q. Yu, H. Jiang, Use of Nutrient rich hydrophytes to create N, P-dually doped porous carbon with robust energy storage performance, Environ. Sci. Technol. 50 (2016) 12421-12428.

[42] W. Zhang, H. Lin, Z. Lin, J. Yin, H. Lu, D. Liu, M. Zhao, 3D hierarchical porous carbon for supercapacitors prepared from lignin through a facile template-free method, ChemSusChem 8 (2015) 2114-2122.

[43] L. Jian, E.H. Liu, W. Li, X.Y. Meng, S.T. Tan, Nickel/carbon nanofibers composite electrodes as supercapacitors prepared by electrospinning, J. Alloly Compounds, 478 (2009) 371-374

[44] J. Li, Q.M. Yang, I. Zhitomirsky, Nickel foam-based manganese dioxide–carbon nanotube composite electrodes for electrochemical supercapacitors, J. Power Sources, 185 (2008) 1569-1574.

[45] Y.Z. Zheng, M.L. Zhang, P. Gao, Preparation and electrochemical properties of multiwalled carbon nanotubes-nickel oxide porous composite for supercapacitors, Mater. Res. Bull, 42(2007) 1740-1747

[46] K. Wang, Y. Cao, X. Wang, P.R. Kharel, W. Gibbons, Nickel catalytic graphitized porous carbon as electrode material for high performance supercapacitors, Energy, 101 (2016) 9-15.

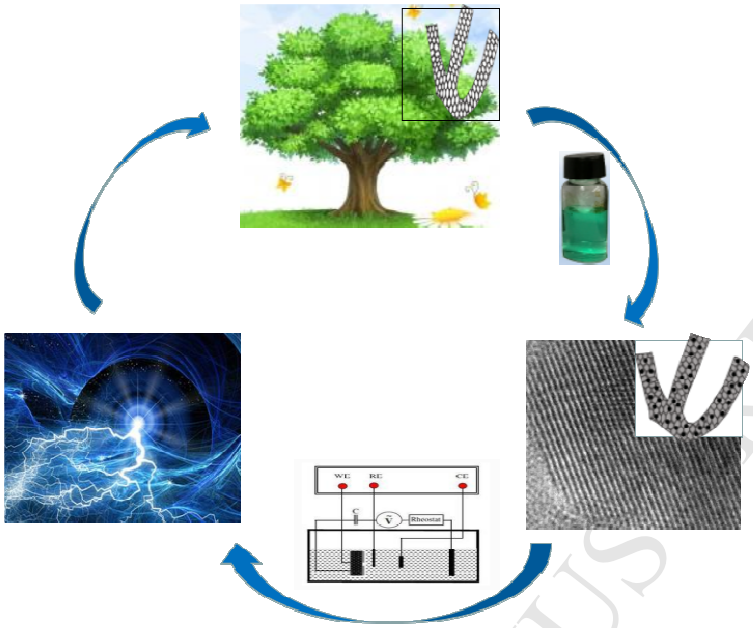

HIGHLIGHTS

- Microstructure of wood was transformed into fiber via papermaking.
- The hybrid carbon fiber is synthesized via electroless decoration and carbonization.
- The as-synthesized carbon fiber exhibits enhanced performance for supercapacitors.